A kinematic-geometric model based on ankles' depth trajectory in frontal plane for gait analysis using a single RGB-D camera

Mehran Hatamzadeh, Laurent Busé, Frédéric Chorin, Pierre Alliez, Jean-Dominique Favreau, Raphael Zory

A kinematic-geometric model based on ankles' depth trajectory in frontal plane for gait analysis using a single RGB-D camera

Mehran Hatamzadeh [a, b, c, *], Laurent Busé [b], Frédéric Chorin [c], Pierre Alliez [b], Jean-Dominique Favreau [d], Raphael Zory [a, c, e]

[a] Université Côte d'Azur, LAMHESS, Nice, France

[b] Université Côte d'Azur, Inria, Sophia Antipolis, France

[c] Université Côte d'Azur, CHU, Cimiez, Plateforme fragilité, Nice, France

[d] EKINNOX Company, Sophia Antipolis, France

[e] Institut Universitaire de France (IUF), Paris, France

[*] **Corresponding Author:** Mehran Hatamzadeh

Address: Université Côte d'Azur, Campus STAPS – Sciences du Sport, 261 Boulevard du Mercantour, 06205 Nice, France.

Phone: +33 676 330 344

E-mail 1: mehran.hatamzadeh@inria.fr

E-mail 2: hatamzadeh.mehran@gmail.com

Abstract:

The emergence of RGB-D cameras and the development of pose estimation algorithms offer opportunities in biomechanics. However, some challenges still remain when using them for gait analysis, including noise which leads to misidentification of gait events and inaccuracy.

Therefore, we present a novel kinematic-geometric model for spatio-temporal gait analysis, based on ankles' trajectory in the frontal plane and distance-to-camera data (depth). Our approach consists of three main steps: identification of the gait pattern and modeling via parameterized curves, development of a fitting algorithm, and computation of locomotive indices. The proposed fitting algorithm applies on both ankles' depth data simultaneously, by minimizing through numerical optimization some geometric and biomechanical error functions.

For validation, 15 subjects were asked to walk inside the walkway of the OptoGait, while the OptoGait and an RGB-D camera (Microsoft Azure Kinect) were both recording. Then, the spatio-temporal parameters of both feet were computed using the OptoGait and the proposed model. Validation results show that the proposed model yields good to excellent absolute statistical agreement ($0.86 \leq R_c \leq 0.99$).

Our kinematic-geometric model offers several benefits: (1) It relies only on the ankles' depth trajectory both for gait events extraction and spatio-temporal parameters' calculation; (2) it is usable with any kind of RGB-D camera or even with 3D marker-based motion analysis systems in absence of toes' and heels' markers; and (3) it enables improving the results by denoising and smoothing the ankles' depth trajectory. Hence, the proposed kinematic-geometric model facilitates the development of portable markerless systems for accurate gait analysis.

Keywords: Kinematic-geometric model, Bézier curve, Ankles' depth trajectory, Spatio-temporal gait analysis, Single RGB-D camera.

1. Introduction

Gait analysis is a way of assessing human walking patterns that can provide relevant quantitative information in the form of gait parameters (Rocha et al., 2018). A complete gait cycle of human consists of two main phases including the stance and the swing phase. In the stance phase, the foot is partially or completely in contact with the walking surface, whereas in the swing phase, there is no contact between them. The possession percentage of each gait phase, gait speed, time and length of step and stride, and cadence are some of the most important gait parameters that are commonly used to study walking patterns in healthy individuals or patients with gait impairments (Latorre et al., 2018; Pantzar-Castilla et al., 2018; Vilas-Boas et al., 2019). Some of the most widely used systems for this purpose include marker-based 3D motion analysis, accelerometry-based tools, and instrumented walkway systems (Klöpfer-Krämer et al., 2020; Petraglia et al., 2019). Despite their high accuracy, they suffer from several disadvantages that lead to lesser usability in clinical environments, as for instance the time-consuming installation of reflective markers, probability of missing markers, requirement of large clinical spaces, unportability, and high costs (Klöpfer-Krämer et al., 2020; Petraglia et al., 2019).

With the fast-paced technological developments, less expensive systems based on RGB and/or RGB-D cameras have emerged; they are portable, markerless, and less intrusive in terms of occupied space, which facilitates their use for clinical applications (Clark et al., 2013; Rocha et al., 2018). However, their accuracy is usually lower than the gold-standard systems, as confirmed by several validation studies (Kanko et al., 2021; Mentiplay et al., 2015; Springer and Seligmann, 2016). Many camera-based gait analysis approaches have been developed, based either on multiple cameras (Sandau et al., 2014) or a single camera (Auvinet et al., 2015; Xu et al., 2015). The state-of-the-art methods utilizing a single camera in the frontal plane are inaccurate, unreliable, and gait events detection in the frontal plane is still a challenging problem in this setting. However, when assessing both feet simultaneously, analyzing in the frontal plane yields better monitoring of gait performance than in the sagittal plane,

since none of the feet hide each other (Clark et al., 2015). Despite the convenience of using a single camera in front, some issues remain, including noise that hampers accurate gait events' detection, lack of heel coordinates, and inaccurate localization of the toe by most of the pose estimation algorithms. These issues lead to mix together some biomechanical parameters by error, lowering the overall accuracy of the gait analysis.

Therefore, this research aims to present and validate a novel kinematic-geometric model for gait analysis, relying only upon distance-to-camera data (depth) and ankles' depth trajectory in the frontal plane. This new approach proceeds in three main steps: (1) Identification of the gait pattern and modeling by parameterized curves, (2) model fitting through optimization, and (3) computation of spatio-temporal gait parameters.

2. Methods

2.1. Participants

Fifteen lower-limb injury-free individuals participated in this research (Age: 26.9±5.5 years old, height: 172.9±8.7 cm, weight: 72.6±17 kg). The study was approved by the local ethics committee and conducted according to the declaration of Helsinki.

2.2. Equipment

A 10-meter long OptoGait system (spatial resolution: 1.041 cm, temporal resolution: 1000 Hz) is used as the reference for validation (Mo Lee et al., 2014; Rudisch et al., 2021). Besides, a single Microsoft Azure Kinect camera is used to acquire ankles' depth data when walking. The camera is placed at 1-meter distance from the end of the OptoGait walkway, at 80 centimeters height, and is set to record at 1920×1080 pixels resolution with 30 frames per second (FPS). The proper depth-

sensing range of this camera is 2-8 meters for the intended purpose. At longer distances, the depth accuracy reduces, and within distances smaller than 2 meters, parts of the body may be out of the sight of the camera.

2.3. Data acquisition

Each subject was asked to walk two times, each at a self-selected pace along the walkway of the OptoGait, while the OptoGait and the RGB-D camera were both recording. The positions of the ankles in each RGB frame were estimated using the *OpenPose*, a 2D human pose estimation algorithm (Cao et al., 2019). Then, 2D position of each ankle, in all frames, was smoothed using Savitzky–Golay low pass filter. Afterward, the ankles' positions for each frame were mapped to the corresponding frame's 3D point cloud, and their depth was extracted. A range of 6 meters length is considered for further analysis out of 10m walking length (2-8m from the camera, corresponding to 3-9m inside the walkway of the OptoGait).

2.4. Proposed approach

The proposed approach proceeds in three main steps. First, the ankles' depth trajectory in the frontal plane and a class of parameterized curves that provide a continuous and sufficiently faithful representation for that trajectory are identified. The number of unknown parameters (control points) of this curve is carefully selected. It must be large enough to take into account the diversity of walking patterns, and meanwhile, small enough to offer resilience to common uncertainties such as measurement noise. Second, the fitting procedure, which adjusts the curve parameters while satisfying the governing constraints, is defined. Third, the locomotor indices are calculated from the fitted curve.

2.4.1. Designing the kinematic-geometric model (Step 1)

When a person walks toward a camera, the ankles' depth decreases and follows a certain pattern in each gait phase which could be considered as a model for the ankles' depth trajectory in a complete gait cycle (Fig.1). Since the gait events are unknown, the complete gait cycle model cannot be used on its own. The only deducible parameter from the ankles' raw depth data is their approximate time and depth in mid-swing/mid-flat foot points. These are the points where both ankles have the same depth and their depth curves intersect each other (Fig.2b). Therefore, each ankle's depth data can be divided into sections where each section ranges from the mid-flat foot point to the next mid-flat-foot point (Fig.2c). Besides, the complete gait cycle model can be modified to adapt to each section. The proposed kinematic-geometric model that can be applied on each section (Fig.2d) consists of three parts: I) A straight line with a zero slope to model from the mid-flat foot to the beginning of the push-off phase, II) a parametric curve to model the push-off, swing, and heel-strike phases. To this end, a Bézier curve of order 3 is utilized to offer flexibility and applicability to different walking patterns. III) A straight line with a zero slope to model from the end of the heel-strike to the mid-flat foot.

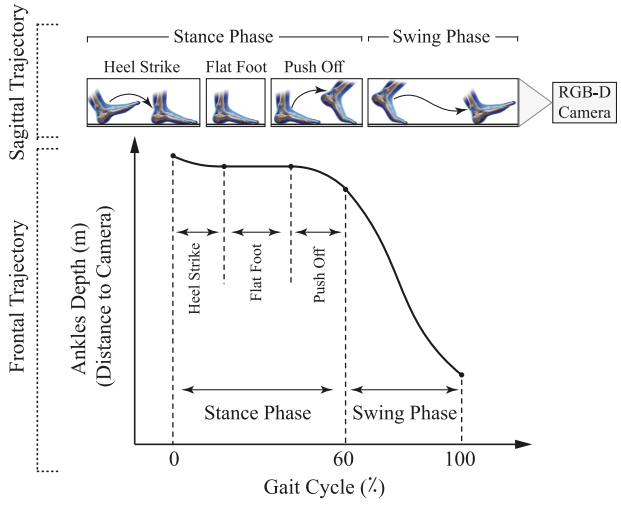

Figure 1- Depth trajectory of the ankle in the frontal plane and corresponding sagittal plane movements in a complete gait cycle. In the heel strike phase, the ankle's depth decreases like a concave upward curve. In the flat foot phase, the ankle's depth remains constant in the corresponding period like a straight line with a zero slope. In the push-off phase, the ankle's depth decreases like a concave downward curve. In the swing phase, there is an increasing speed until the mid-swing and then decreasing speed, like a curve that switches its acceleration sign in the middle.

2.4.1.1. Bézier curves

Bézier curves are parametric curves that define a smooth pattern between two points (Prautzsch et al., 2002; Shao and Zhou, 1996). The curvature between these two points is adjusted by some control points whose cardinality exceeds the order by one (Walton and Meek, 1996). The complete form of the cubic Bézier curve (*B(u)*) and its first derivative (*B'(u)*) is as follows:

$$\begin{aligned} &B(u) = (1-u)^3 P_0 + 3u(1-u)^2 P_1 + 3u^2(1-u)P_2 + u^3 P_3 \quad , \quad P_i = \begin{pmatrix} x_i \\ y_i \end{pmatrix} \quad , \quad 0 \le u \le 1 \\ &B'(u) = 3(1-u)^2(P_1 - P_0) + 6u(1-u)(P_2 - P_1) + 3u^2(P_3 - P_2) \end{aligned} \tag{1}$$

where u denotes the parameter and P_i is the i^{th} control point (Farouki, 2012). According to the definition, $B(0)=P_0$, $B(1)=P_3$, i.e., the first and last control points are the beginning and the endpoint of the curve respectively. Furthermore, $B'(0) = 3(\overrightarrow{P_0P_1})$ and $B'(1) = 3(\overrightarrow{P_2P_3})$. Therefore, restrictive conditions (Eq.2) are added to maintain the geometric continuity (G1) of the model, meaning that both tangent lines coincide at the connecting points of the Bézier curve and lines.

$$G1 \;\; Conditions: \begin{cases} Y_{Line1} = y_0 = y_1 \\ Y_{Line2} = y_2 = y_3 \end{cases} \tag{2}$$

2.4.2. Optimization and fitting algorithm (Step 2)

The kinematic-geometric model is fitted to the depth data of the ankles by minimizing an objective function comprising the geometric error terms and the events error term.

2.4.2.1. Geometric error

The geometric error is defined by the orthogonal distance from each depth sample to the kinematic-geometric model. To compute it, first, the area to which each sample belongs is defined and then, the orthogonal distance is calculated according to this area. Assuming that the depth samples in each section are $\{(X_1, Y_1), \ldots, (X_N, Y_N)\}$, consisting of N samples, two values are defined as follows: A is the number of samples whose occurrence time is before the time of the first control point (x_0) and

belong to the line 1 area, while *C* is the number of samples whose occurrence time lies between the time of the first (x_0) and the last (x_3) control points which belong to the Bézier curve area. Consequently, *N-(A+C)* is equal to the number of samples whose occurrence time is after the time of the last control point (x_3) and belong to the line 2 area. To find the orthogonal distance of a sample in the Bézier curve area, a point on the Bézier curve called the orthogonal projection point (*B(v)*) is computed such that the vector connecting the orthogonal projection point to that sample is perpendicular to the Bézier curve at *v* (Wang et al., 2006). To do so, the roots of Eq.3, which is a degree 5 univariate polynomial in *v*, should be found. The corresponding *v* value for the orthogonal projection point of each sample in the Bézier curve area is the root that has a real part in the range [0-1] and zero imaginary part. After finding the *v* value, the coordinates of the orthogonal projection point are found by evaluating the Bézier curve at *v*.

$$(\overrightarrow{B'(v)}) \cdot (\overrightarrow{\begin{pmatrix} X_j \\ Y_j \end{pmatrix} - B(v)}) = 0 \quad , \quad j = A+1, A+2, ..., A+C \quad , \quad 0 \le v \le 1 \tag{3}$$

where *B(v)* is the Bézier curve, *B'(v)* is its first derivative, and *v* is the parameter that provides the orthogonal projection point for the j^{th} depth sample in the Bézier curve area. The sum of the error of the samples in line 1 area (*E1*), in the Bézier curve area (*E2*), and in line 2 area (*E3*) is the geometric error term for one section, which is as follows:

$$\begin{aligned} E1 &= \sum_{j=1}^{A} (Y_{Line1} - Y_j)^2 && \text{if} \quad X_j < x_0 \\ E2 &= \sum_{j=A+1}^{A+C} \left\| B(v) - \overrightarrow{\begin{pmatrix} X_j \\ Y_j \end{pmatrix}} \right\|_2^2 && \text{if} \quad x_0 \le X_j \le x_3 \\ E3 &= \sum_{j=A+C+1}^{N} (Y_{Line2} - Y_j)^2 && \text{if} \quad X_j > x_3 \\ E_{Geometric} &= E1 + E2 + E3 \end{aligned} \tag{4}$$

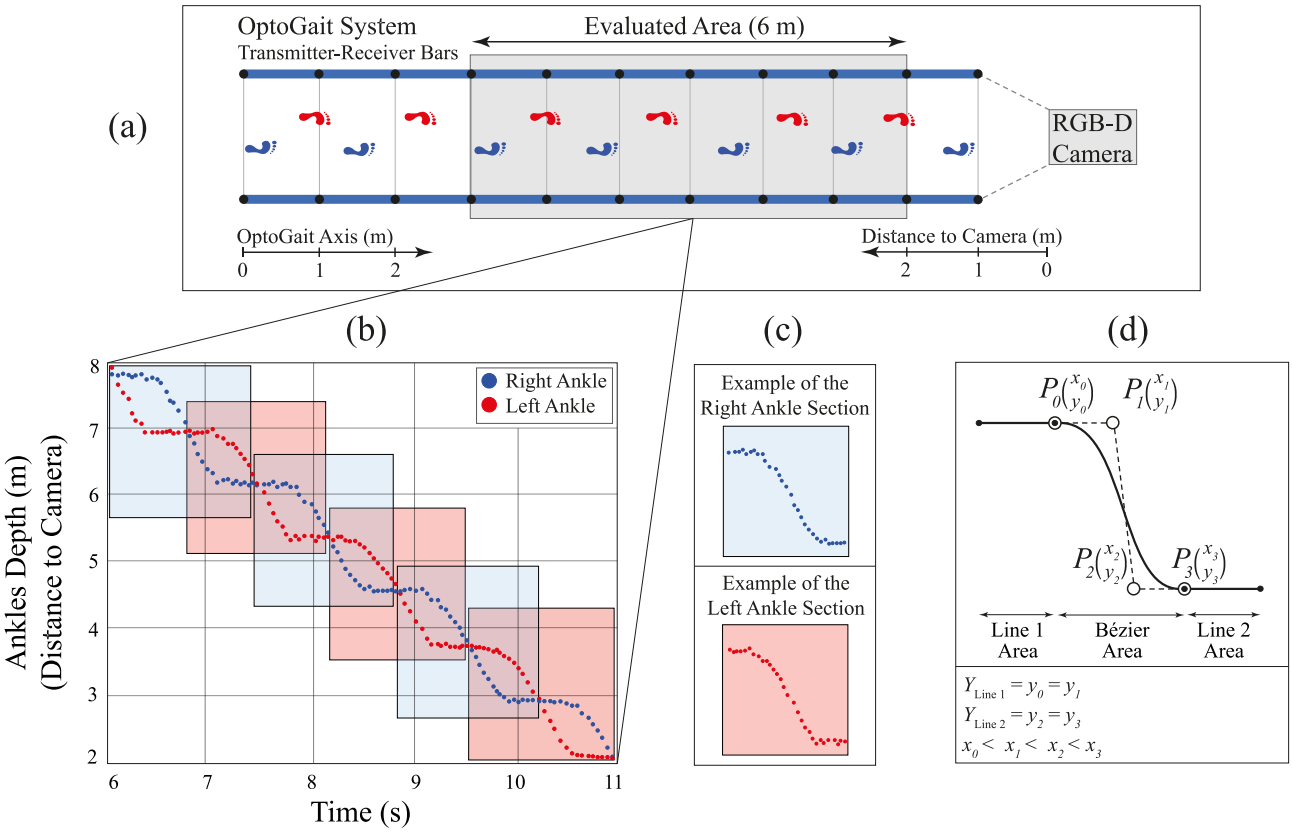

Figure 2- (a) Data acquisition procedure using the OptoGait and the RGB-D camera (b) Ankles' raw depth data when walking toward a camera. Intersection points are the local minima of the difference between the two curves. (c) Example of a section for each ankle, representing the data from mid-flat foot to mid-flat foot. (d) Proposed kinematic-geometric model for each section. Empty black circles depict the cubic Bézier curve's control points (P_i), the dashed line connecting the control points is the control polygon of the curve, and filled black circles depict the starting and ending points of the lines.

2.4.2.2. Events error

The second term of error is based on the time difference in gait events of both feet that are considered to match each other. According to the literature, if the movement variation of the ankle relative to a fixed point on the body (e.g., sacrum or center of mass) is calculated, then the horizontal component for the ankle's velocity changes sign at initial contact and beginning of the swing phase (Zeni et al., 2008). This approach is generalized as follows: At all intersection points, which are the mid-swing/mid-flat-foot moments, the sacrum is at a fixed distance (horizontally) from the depth of the ankles. Therefore, the line passing through all intersection points is parallel to the horizontal axis of the sacrum's movement. Hence, this interpolated line ($\overrightarrow{IL}$) can be utilized as an approximation for the

sacrum's trajectory, assuming constant speed and minor movement variations. In other words, $\overrightarrow{IL}$ depicts the depth trajectory of a fixed part of the body that becomes closer to the camera with constant speed (Fig.3b). Therefore, the extrema of the Bézier curves relative to $\overrightarrow{IL}$ reveal the gait events, where the ankles' velocity sign changes. The extrema of each Bézier curve relative to $\overrightarrow{IL}$ (Fig.3c) are the points on the curve (*B(w)*), obtained by solving Eq.5, which is a quadratic univariate polynomial in *w*. In other words, these extrema are the roots of Eq.5 that have a real part in the range [0-1] and zero imaginary part.

$$\overrightarrow{B'(w)} \times \overrightarrow{IL} = 0 \quad , \quad 0 \le w \le 1 \tag{5}$$

where *w* denotes the Bézier curve's parameter where the tangent vector to the Bézier curve is parallel to $\overrightarrow{IL}$, so it provides the extrema of the curves relative to $\overrightarrow{IL}$. As shown in Fig.3c, between each two consecutive intersection points, the extremum of the Bézier curve that corresponds to the anterior ankle (closer in depth) indicates the initial contact point and at that point, the posterior ankle (further away in depth) should be at the end of flat foot phase. Hence, the time of endpoint of line 1 in the posterior ankles' model should match the time of the second extremum of the anterior ankle's Bézier curve model. The time difference between them is the detection error for the initial contact time, which is as follows:

$$E_{Initial\ \ Contact} = \left(x_0^{Posterior} - Time(B(w)^{Anterior}) \right)^2 \tag{6}$$

In addition, the extremum of the Bézier curve that corresponds to the posterior ankle indicates the beginning of the swing and at that point, the anterior ankle should be at the beginning of the flat foot phase. Hence, the time of the first extremum of the posterior ankle's Bézier curve model should match the time of starting point of Line 2 in the anterior ankle's model. The time difference between them is the detection error for the starting time of the swing, which is as follows:

$$E_{Swing} = \left(x_3^{Anterior} - Time(B(w)^{Posterior}) \right)^2 \tag{7}$$

The events error term in between each two consecutive intersection points is defined by the sum of $E_{Initial\ Contact}$ and E_{Swing}.

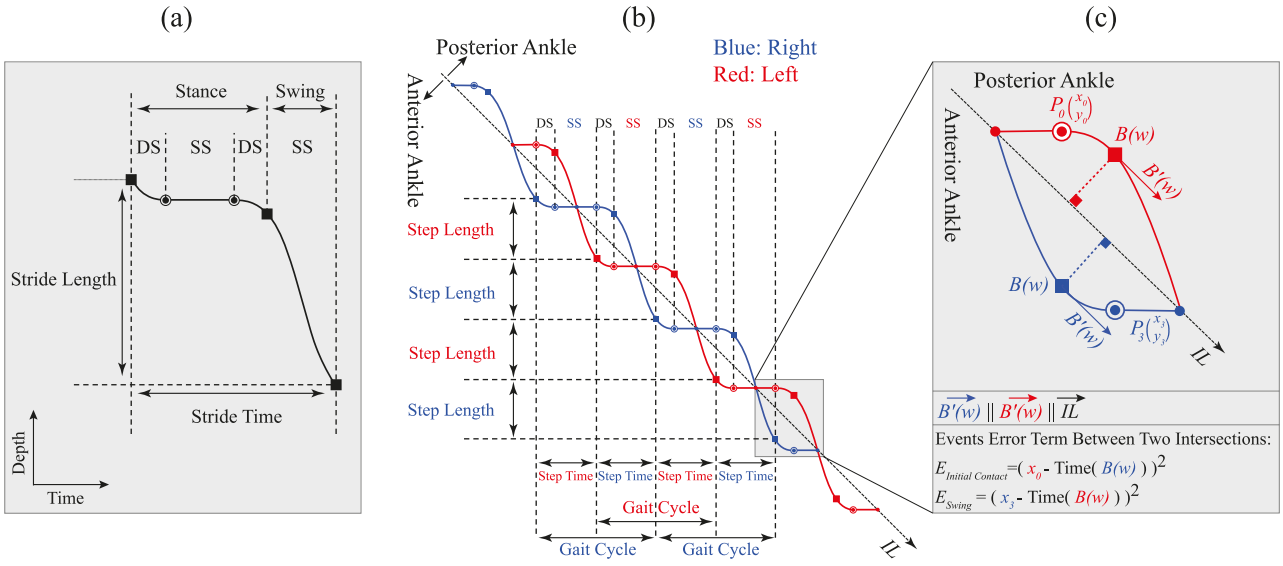

Figure 3- (a) Extraction of the complete gait cycle model from the result of applying the proposed kinematic-geometric model to the ankles' depth data and the way of computing gait parameters. (b) Kinematic-geometric model fitted to the ankles' depth data. (c) Events error term between two consecutive intersection points. DS refers to the double support, SS refers to the single support, the interpolated line is IL in dashed black color, filled squares depict the extremities relative to the IL, empty circles depict the first and last control points of the Bézier curves, and filled circles indicate the starting and ending point of the lines.

To generalize the presented approach on all sections of one ankle, Y_{Line2} in one section's model should be equal to Y_{Line1} of the next section's model. By doing so, the model can be applied to all depth data of each ankle, yielding a complete continuous representation (Fig.3b). To do so, in each iteration of the optimization, first the geometric error in all sections of the left and the right ankle is calculated and is normalized by their geometric error value at initial answer. Then, the line passing through all intersection points is found and the extrema of the curves relative to this line are calculated. Afterward, the events error term between each two consecutive intersection points is calculated and normalized by the events error value at initial answer. The total error function is as follows:

$$Total \quad Error = \frac{\sum_{Left\ \ Ankle}^{Sections} E_{Geometric}}{E0_{Left}} + \frac{\sum_{Right\ \ Ankle}^{Sections} E_{Geometric}}{E0_{Right}} + \frac{\sum^{Intersections} \left(\overbrace{E_{Initial\ \ Contact} + E_{Swing}}^{Between\ \ Two\ \ Consecutive\ \ Intersection} \right)}{E0_{Events}} \tag{8}$$

Where $E0_{Left}$ and $E0_{Right}$ are the geometric error values in all sections of the left and the right ankle at initial answer, and $E0_{Events}$ is the value of events error term in all intersections at initial answer that are used for normalization. According to the quadratic error functions and the governing constraints, sequential quadratic programming (SQP) is used for fitting (Nocedal and Wright, 2006). SQP is an iterative optimization algorithm for mathematical problems whose objective function and the constraints are twice continuously differentiable. In the SQP, first, a Lagrangian is formed by combining the objective function and the constraints into a single Lagrangian function through Lagrange multipliers. Then, a sequence of optimization subproblems is formed in each iteration that corresponds to the quadratic approximation of the objective function with linearized constraints. These subproblems are solved by quadratic programming (QP), considering the Karush–Kuhn–Tucker optimality conditions to assess the feasibility. This cyclic process continues until the convergence to a minimum of the objective function.

2.4.3. Locomotor indices calculations (Step 3)

Following the simultaneous fitting of the model on both ankles' depth data, spatio-temporal parameters can be calculated as illustrated in Fig.3.

To validate the model, on one hand, spatio-temporal gait parameters within the walking range of 6 meters have been calculated using the OptoGait. On the other hand, spatio-temporal parameters have been calculated in the same walking area using the acquired depth data and the proposed model.

2.5. Statistics

To assess statistical agreement between the proposed method and the OptoGait, first, a one-sample t-test is used to assess whether the difference in each parameter is distinguishable from zero or not (Vilas-Boas et al., 2019). The agreement is then assessed visually using the Bland-Altman method with 95% limits of agreement (LoA) (Clark et al., 2013). Pearson's correlation for relative agreement and Lin's concordance correlation with associated 95% confidence intervals (CI) for absolute agreement is used (Clark et al., 2013; Mentiplay et al., 2015). Correlation thresholds were set as poor (<0.5), moderate (≥0.5 and <0.75), good (≥0.75 and <0.9), and excellent (≥0.9) (Vilas-Boas et al., 2019). Further, percentage error (PE%) is computed using the standard deviation of the difference and the mean, representing the percentage of bias relative to the mean of the measurements (Clark et al., 2013).

3. Results

For all calculated parameters, the t-tests' results were not significant and hence, the agreement was assessed using its corresponding methods. Descriptive statistics for the agreements are outlined in Table 1. Statistical agreement between the results of the OptoGait and the proposed model was excellent for the overall values of all spatio-temporal parameters ($R \geq 0.9$ and $R_c \geq 0.9$). For the right foot, the swing percentage yields excellent relative agreement ($R=0.9$) and good absolute agreement ($R_c=0.87$). The rest of the parameters for the right foot yield excellent relative and absolute agreement. For the left foot, absolute agreement in step time ($R_c=0.89$), stance phase percentage ($R_c=0.89$), and swing phase percentage ($R_c=0.86$) was good and the other parameters yield excellent absolute agreement. Bland Altman plot of some overall parameters are illustrated in Fig.4. Among all the assessed parameters, gait speed, stride time, and stride length exhibit the highest agreements. Percentage errors between the measurements for all the parameters were ranging between 1.54% and 6.56%.

Table 1. Mean and standard deviation (SD) of gait parameters for both left and right foot as well as their overall value obtained from the proposed method and the OptoGait, mean difference with 95% LoA, percentage error (PE%), Pearson's correlation coefficient (R), and Lin's concordance correlation coefficient (R_c) with associated 95% CI. All correlations were statistically significant ($p<0.05$).

Parameter		Mean (± SD) Proposed Method	Mean (± SD) OptoGait	Mean Difference (95% LoA)	PE%	R	R_c (95%CI)
Step Time (s)	Left	0.549 (0.039)	0.55 (0.037)	0.00005 (-0.032 to 0.032)	5.99%	0.91	0.89 (0.82 to 0.96)
	Right	0.547 (0.047)	0.546 (0.04)	0.0015 (-0.033 to 0.036)	6.56%	0.92	0.9 (0.84 to 0.96)
	Overall	0.548 (0.038)	0.547 (0.036)	0.0012 (-0.011 to 0.013)	2.33%	0.98	0.98 (0.97 to 0.99)
Step Length (m)	Left	0.737 (0.059)	0.733 (0.061)	0.0045 (-0.022 to 0.031)	3.75%	0.97	0.96 (0.94 to 0.98)
	Right	0.724 (0.064)	0.723 (0.056)	0.0015 (-0.044 to 0.047)	6.47%	0.93	0.91 (0.86 to 0.96)
	Overall	0.731 (0.055)	0.728 (0.054)	0.003 (-0.015 to 0.021)	2.50%	0.98	0.98 (0.97 to 0.99)
Stride Time (s)	Left	1.097 (0.081)	1.094 (0.072)	0.003 (-0.031 to 0.037)	3.18%	0.98	0.97 (0.95 to 0.99)
	Right	1.097 (0.077)	1.093 (0.069)	0.004 (-0.032 to 0.04)	3.40%	0.97	0.96 (0.93 to 0.99)
	Overall	1.097 (0.078)	1.094 (0.071)	0.0035 (-0.022 to 0.029)	2.38%	0.98	0.98 (0.97 to 0.99)
Stride Length (m)	Left	1.461 (0.106)	1.459 (0.107)	0.003 (-0.033 to 0.039)	2.54%	0.98	0.98 (0.97 to 0.99)
	Right	1.467 (0.117)	1.460 (0.104)	0.007 (-0.054 to 0.068)	4.30%	0.96	0.95 (0.92 to 0.98)
	Overall	1.464 (0.111)	1.459 (0.105)	0.005 (-0.035 to 0.045)	2.81%	0.98	0.98 (0.97 to 0.99)
Gait Speed (ms^{-1})	Left	1.342 (0.162)	1.339 (0.147)	0.0025 (-0.04 to 0.045)	3.24%	0.99	0.99 (0.98 to 0.99)
	Right	1.344 (0.155)	1.342 (0.148)	0.0015 (-0.031 to 0.034)	2.48%	0.99	0.99 (0.98 to 0.99)
	Overall	1.343 (0.158)	1.341 (0.147)	0.002 (-0.027 to 0.031)	2.23%	0.99	0.99 (0.98 to 0.99)
Cadence (steps/minute)	Left	109.971 (8.023)	110.104 (7.141)	-0.132 (-3.341 to 3.076)	2.97%	0.98	0.97 (0.95 to 0.99)
	Right	109.835 (7.550)	110.539 (7.309)	-0.704 (-4.634 to 3.225)	3.64%	0.96	0.94 (0.91 to 0.98)
	Overall	109.903 (7.712)	110.322 (7.203)	-0.418 (-2.803 to 1.966)	2.21%	0.99	0.98 (0.97 to 0.99)
Stance Phase (%)	Left	58.744 (1.908)	58.851 (1.824)	-0.106 (-1.664 to 1.45)	2.70%	0.91	0.89 (0.82 to 0.96)
	Right	58.571 (2.068)	58.72 (1.861)	-0.149 (-1.539 to 1.241)	2.41%	0.94	0.92 (0.87 to 0.97)
	Overall	58.657 (1.489)	58.824 (1.581)	-0.166 (-1.055 to 0.723)	1.54%	0.95	0.94 (0.90 to 0.98)
Swing Phase (%)	Left	41.255 (1.908)	41.161 (1.806)	0.093 (-1.628 to 1.815)	4.26%	0.88	0.86 (0.78 to 0.94)
	Right	41.428 (2.068)	41.286 (1.848)	0.142 (-1.562 to 1.847)	4.20%	0.90	0.87 (0.80 to 0.94)
	Overall	41.342 (1.489)	41.197 (1.556)	0.144 (-1.020 to 1.310)	2.88%	0.92	0.90 (0.84 to 0.96)

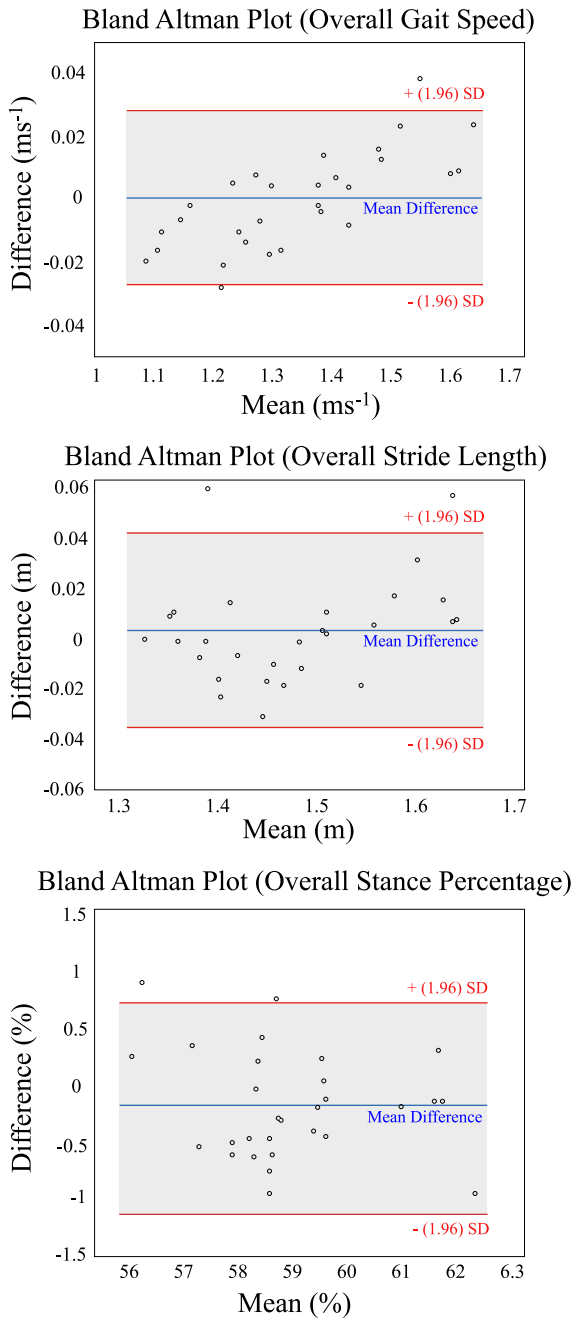

Figure 4- Bland Altman plot with 95% LoA (red lines) and mean difference (blue line) for the overall gait speed, the overall stride length, and the overall stance phase percentage.

4. Discussion

The objective of this research was to introduce and validate a novel kinematic-geometric model based on the ankles' depth trajectory for spatio-temporal gait analysis using a single RGB-D camera. The proposed model yields good to excellent absolute statistical agreement ($0.86 \leq R_c \leq 0.99$) in spatio-temporal parameters compared to the OptoGait system. In terms of the percentage error (PE%) of the

overall parameters, the PEs% of 2.33%, 2.5%, 2.38%, 2.81%, and 2.23% was achieved in this study for step time, step length, stride time, stride length, and gait speed respectively. This is while, previous studies reported PEs% up to 19%, 5%, 16%, 3%, and 8% in the overall value of the above-mentioned parameters with weaker agreements than the results of this study (Clark et al., 2013, Clark et al., 2015; Mentiplay et al., 2015; Vilas-Boas et al., 2019). The main reasons for achieving higher accuracy using the proposed model are such that, firstly, it denoises and smooths the data by fitting the model on them; Secondly, it takes into account both ankles' depth position to detect gait events which reduces the probability of events misidentification. It should be noted that the obtained final accuracy is the product of several steps, each of which may influence the results. The first factor is the camera and its depth-sensing technology (Tölgyessy et al., 2021; Vilas-Boas et al., 2019; Yeung et al., 2021). The second factor is the accuracy of the human pose estimation algorithm (Clark et al., 2019; Zago et al., 2020). The third factor is the color of clothes and shoes, which can trap the skeleton tracking algorithm. However, to make the results more realistic, the subjects were not asked to wear special shoes or clothes in this study. The existence of noise in joints' 3D position, as well as the final accuracy in identifying anatomical landmarks, could be related to the above-mentioned factors (Albert et al., 2020). The fourth factor is the FPS rate of the camera, which usually fluctuates. Low FPS may result in an inaccurate final pattern and manifests itself more in fast motions where the number of depth samples that fall in each section and the proposed model should be applied on, is low.

This study had some limitations. First, the presented approach is only validated on healthy individuals. Second, due to the limitations of the camera, only 6 meters of walking distance is considered for validation. Third, due to the systematic bias of the OptoGait in calculating single and double support phase percentages (Lee et al., 2014; Lienhard et al., 2013; Mo Lee et al., 2014; Rudisch et al., 2021), these parameters have not been assessed in this research. However, as shown in Fig.3, they can be also extracted from the proposed model.

Conclusion

The first benefit of the proposed kinematic-geometric model is that it only uses the ankles' depth data to extract gait events, without requiring other joints' trajectories. Second, other types of RGB-D cameras or pose estimation algorithms can also be utilized. Third, it can be applied not only to the ankles' depth data acquired from the front view, but also to data acquired from the back view of the subject (e.g., the output of two synchronized cameras, in the front and in the back). Fourth, utilization of the cubic Bézier curve enables obtaining different patterns based on the control points' locations, opening the door to the applicability to various pathologies. In summary, the proposed model facilitates the development of markerless, and portable systems for accurate gait analysis with a single RGB-D camera.

Declaration of competing interest

The authors have no financial, professional, or personal interest of any nature of kind that could be construed as a potential conflict of interest or could be influencing the presented content.

Acknowledgments

The authors would like to acknowledge EKINNOX company for their technical contribution in data acquisition stage. It is worth mentioning that their contribution does not bring ownership rights to them.

Funding

This research belongs to the project MoVE-IT, funded in the framework of the COFUND BoostUrCAreer program of the Université Côte d'Azur. This program has received funding from the European Union's Horizon 2020 research and innovation programme under the Marie Sklodowska-Curie Actions (MSCA, Grant Number: 847581), the Conseil Region SUD Provence-Alpes-Côte d'Azur, and the IDEX UCA^{JEDI}.

References

Albert, J.A., Owolabi, V., Gebel, A., Brahms, C.M., Granacher, U., Arnrich, B., 2020. Evaluation of the pose tracking performance of the azure kinect and kinect v2 for gait analysis in comparison with a gold standard: A pilot study. Sensors 20(18), 1–22. https://doi.org/10.3390/s20185104

Auvinet, E., Multon, F., Aubin, C.E., Meunier, J., Raison, M., 2015. Detection of gait cycles in treadmill walking using a Kinect. Gait and Posture 41(2), 722–725. https://doi.org/10.1016/j.gaitpost.2014.08.006

Cao, Z., Hidalgo, G., Simon, T., Wei, S.-E., Sheikh, Y., 2019. OpenPose: Realtime Multi-Person 2D Pose Estimation using Part Affinity Fields. IEEE transactions on pattern analysis and machine intelligence 43(1), 172–186. https://doi.org/10.1109/TPAMI.2019.2929257

Clark, R.A., Bower, K.J., Mentiplay, B.F., Paterson, K., Pua, Y.H., 2013. Concurrent validity of the Microsoft Kinect for assessment of spatiotemporal gait variables. Journal of Biomechanics 46(15), 2722–2725. https://doi.org/10.1016/j.jbiomech.2013.08.011

Clark, R.A., Mentiplay, B.F., Hough, E., Pua, Y.H., 2019. Three-dimensional cameras and skeleton pose tracking for physical function assessment: A review of uses, validity, current developments and Kinect alternatives. Gait and Posture. https://doi.org/10.1016/j.gaitpost.2018.11.029

Clark, R.A., Vernon, S., Mentiplay, B.F., Miller, K.J., McGinley, J.L., Pua, Y.H., Paterson, K., Bower, K.J., 2015. Instrumenting gait assessment using the Kinect in people living with stroke: reliability and association with balance tests. Journal of neuroengineering and rehabilitation 12(Article 15). https://doi.org/10.1186/s12984-015-0006-8

Farouki, R.T., 2012. The Bernstein polynomial basis: A centennial retrospective. Computer Aided Geometric Design. https://doi.org/10.1016/j.cagd.2012.03.001

Kanko, R.M., Laende, E., Selbie, W.S., Deluzio, K.J., 2021. Inter-session repeatability of markerless motion capture gait kinematics. Journal of Biomechanics 121(Article 110422). https://doi.org/10.1016/j.jbiomech.2021.110422

Klöpfer-Krämer, I., Brand, A., Wackerle, H., Müßig, J., Kröger, I., Augat, P., 2020. Gait analysis – Available platforms for outcome assessment. Injury 51(Supplement 2), S90–S96. https://doi.org/10.1016/j.injury.2019.11.011

Latorre, J., Llorens, R., Colomer, C., Alcañiz, M., 2018. Reliability and comparison of Kinect-based methods for estimating spatiotemporal gait parameters of healthy and post-stroke individuals. Journal of Biomechanics 72(27 April), 268–273. https://doi.org/10.1016/j.jbiomech.2018.03.008

Lee, M., Song, C., Lee, K., Shin, D., Shin, S., 2014. Agreement between the spatio-temporal gait parameters from treadmill-based photoelectric cell and the instrumented treadmill system in healthy young adults and stroke patients. Medical Science Monitor 20, 1210–1219. https://doi.org/10.12659/MSM.890658

Lienhard, K., Schneider, D., Maffiuletti, N.A., 2013. Validity of the Optogait photoelectric system for the assessment of spatiotemporal gait parameters. Medical Engineering and Physics 35(4), 500–504. https://doi.org/10.1016/j.medengphy.2012.06.015

Mentiplay, B.F., Perraton, L.G., Bower, K.J., Pua, Y.H., McGaw, R., Heywood, S., Clark, R.A., 2015. Gait assessment using the Microsoft Xbox One Kinect: Concurrent validity and inter-day reliability of spatiotemporal and kinematic variables. Journal of Biomechanics 48(10), 2166–2170. https://doi.org/10.1016/j.jbiomech.2015.05.021

Mo Lee, M., ho Song, C., Jin Lee, K., Woo Jung, S., ChuL Shin, D., ho Shin, S., 2014. Concurrent Validity and Test-retest Reliability of the OPTOGait Photoelectric Cell System for the Assessment of Spatio-temporal Parameters of the Gait of Young Adults. Journal of Physical Therapy Science 26(1), 81–85. https://doi.org/10.1589/jpts.26.81

Nocedal, J., Wright, S.J., 2006. Sequential Quadratic Programming. Numerical optimization, 529–562. Springer New York, NY. https://doi.org/10.1007/978-0-387-40065-5

Pantzar-Castilla, E., Cereatti, A., Figari, G., Valeri, N., Paolini, G., della Croce, U., Magnuson, A., Riad, J., 2018. Knee joint sagittal plane movement in cerebral palsy: a comparative study of 2-dimensional markerless video and 3-dimensional gait analysis. Acta Orthopaedica 89(6), 656–661. https://doi.org/10.1080/17453674.2018.1525195

Petraglia, F., Scarcella, L., Pedrazzi, G., Brancato, L., Puers, R., Costantino, C., 2019. Inertial sensors versus standard systems in gait analysis: A systematic review and meta-analysis. European Journal of Physical and Rehabilitation Medicine. https://doi.org/10.23736/S1973-9087.18.05306-6

Prautzsch, H., Boehm, W., Paluszny, M., 2002. Bézier and B-Spline Techniques. Springer Berlin, Heidelberg. https://doi.org/10.1007/978-3-662-04919-8

Rocha, A.P., Choupina, H.M.P., Vilas-Boas, M. do C., Fernandes, J.M., Cunha, J.P.S., 2018. System for automatic gait analysis based on a single RGB-D camera. PLoS ONE 13(8). https://doi.org/10.1371/journal.pone.0201728

Rudisch, J., Jöllenbeck, T., Vogt, L., Cordes, T., Klotzbier, T.J., Vogel, O., Wollesen, B., 2021. Agreement and consistency of five different clinical gait analysis systems in the assessment of spatiotemporal gait parameters. Gait and Posture 85(March), 55–64. https://doi.org/10.1016/j.gaitpost.2021.01.013

Sandau, M., Koblauch, H., Moeslund, T.B., Aanæs, H., Alkjær, T., Simonsen, E.B., 2014. Markerless motion capture can provide reliable 3D gait kinematics in the sagittal and frontal plane. Medical Engineering and Physics 36(9), 1168–1175. https://doi.org/10.1016/j.medengphy.2014.07.007

Shao, L., Zhou, H., 1996. Curve Fitting with Bézier Cubics. Graphical Models and Image Processing 58(3), 223–232. https://doi.org/10.1006/gmip.1996.0019

Springer, S., Seligmann, G.Y., 2016. Validity of the kinect for gait assessment: A focused review. Sensors 16(2). https://doi.org/10.3390/s16020194

Tölgyessy, M., Dekan, M., Chovanec, L., 2021. Skeleton tracking accuracy and precision evaluation of Kinect V1, Kinect V2, and the azure kinect. Applied Sciences 11(12), 5756. https://doi.org/10.3390/app11125756

Vilas-Boas, M.D.C., Choupina, H.M.P., Rocha, A.P., Fernandes, J.M., Cunha, J.P.S., 2019. Full-body motion assessment: Concurrent validation of two body tracking depth sensors versus a gold standard system during gait. Journal of Biomechanics 87(18 April), 189–196. https://doi.org/10.1016/j.jbiomech.2019.03.008

Vilas-Boas, M.D.C., Rocha, A.P., Choupina, H.M.P., Cardoso, M.N., Fernandes, J.M., Coelho, T., Cunha, J.P.S., 2019. Validation of a single RGB-D camera for gait assessment of polyneuropathy patients. Sensors 19(22), 4929. https://doi.org/10.3390/s19224929

Walton, D.J., Meek, D.S., 1996. A planar cubic Bézier spiral. Journal of Computational and Applied Mathematics 72(1), 85–100. https://doi.org/10.1016/0377-0427(95)00246-4

Wang, W., Pottmann, H., Liu, Y., 2006. Fitting B-Spline Curves to Point Clouds by Curvature-Based Squared Distance Minimization. ACM Transactions on Graphics (ToG) 25(2), 214–238. https://doi.org/10.1145/1138450.1138453

Xu, X., McGorry, R.W., Chou, L.S., Lin, J. hua, Chang, C. chi, 2015. Accuracy of the Microsoft Kinect™ for measuring gait parameters during treadmill walking. Gait and Posture 42(2), 145–151. https://doi.org/10.1016/j.gaitpost.2015.05.002

Yeung, L.F., Yang, Z., Cheng, K.C.C., Du, D., Tong, R.K.Y., 2021. Effects of camera viewing angles on tracking kinematic gait patterns using Azure Kinect, Kinect v2 and Orbbec Astra Pro v2. Gait and Posture 87 (June), 19–26. https://doi.org/10.1016/j.gaitpost.2021.04.005

Zago, M., Luzzago, M., Marangoni, T., de Cecco, M., Tarabini, M., Galli, M., 2020. 3D Tracking of Human Motion Using Visual Skeletonization and Stereoscopic Vision. Frontiers in Bioengineering and Biotechnology 8, 181. https://doi.org/10.3389/fbioe.2020.00181

Zeni, J.A., Richards, J.G., Higginson, J.S., 2008. Two simple methods for determining gait events during treadmill and overground walking using kinematic data. Gait and Posture 27(4), 710–714. https://doi.org/10.1016/j.gaitpost.2007.07.007